Characterization of a Dual-Polarized Connected-Dipole Array for Ku-Band Mobile Terminals

Bolt, RJ; Cavallo, D; Gerini, G; Deurloo, D; Grooters, G; Neto, A; Toso, G

DOI
10.1109/TAP.2015.2509505

Publication date
2016

Document Version
Accepted author manuscript

Published in
IEEE Transactions on Antennas and Propagation

Characterization of a Dual-Polarized Connected-Dipole Array for Ku-Band Mobile Terminals

Roland J. Bolt, Daniele Cavallo, *Member, IEEE,* Giampiero Gerini, *Senior Member, IEEE,* Duije Deurloo, Reindert Grooters, Andrea Neto, *Fellow, IEEE,* and Giovanni Toso, *Senior Member, IEEE*

***Abstract*— In this paper we present the characterization of a Ku-band connected-dipole array for mobile Satcom application. The prototype array consists of 2×256 dipole radiators arranged in a square grid, to form 16×16 dual-polarized cells. It has been designed to operate over a wide band ranging from 10.7 to 14.5 GHz (30%), accommodating in a single antenna both the transmit (14.0 to 14.5 GHz) and the receive (10.70 to 12.75 GHz) bands for the application. The array has been characterized in terms of active reflection (AR) and radiation patterns. Dedicated test support equipment (TSE) has been developed and used to test the array radiation characteristics. Over the frequency range of operation, the array maintains good matching (ensuring system gain to noise temperature better than 8 dB/K) and good radiation performance while scanning as far as 60° in all the azimuth planes. The cross-polarization suppression is better than 15 dB within most of the scan range and reaches 10 dB for the extreme scan angles in the diagonal plane.**

***Index Terms*— Connected arrays, dual polarization, satellite communication, ultra-wideband arrays, wide-scanning arrays.**

I. Introduction

For quite some years now interest has been directed to mobile terminals utilizing broadband services provided by satellites. Especially the aeronautical sector has gained significant attention, where broadband Internet access for passengers on-board of aircraft is expected to have a large market potential. Where previously a low (kbps) data rate communication service with quasi-global coverage was available, the currently available services provide larger coverage and high (Mbps) data rate links to be utilized. In-flight entertainment is one such communication service appealing to airline operators, requiring a high data rate link [1]. The prototype array discussed in this paper relates to this application. The general idea is to use TV-satellites having reached their end-of-life while still in good technical state for the service and to provide the necessary coverage. In-flight entertainment therefore makes use of the Ku-band, i.e.: 10.70 to 12.75 GHz for receive and 14.0 to 14.5 GHz for transmit and requires dual-polarized capability.

For airborne platforms like airliners, a full hemispherical coverage of the antenna main beam becomes necessary. Even more: scanning surpassing the 90° from zenith is required to account for pitch and roll of the aircraft [2]. Several antenna architectural solutions to provide this coverage have been studied. One example is presented in [3] and consists of a quasi-hemispherical array measuring 39 cm in height and 84 cm in diameter. Beam scanning relies on activating that portion of the array that is facing the satellite. Another configuration with six antenna panels, with one oriented to zenith, is explored in [1]. Despite the fact that such a solution would relax the requirement for the maximum scanning angle per panel, it is considered, like the hemispherical solution, to have too much impact on the aircraft fuselage, aerodynamics, and electrical and mechanical complexity.

For these reasons, in this work we present the development of a single antenna panel capable of electronic scanning to 60° conically. The hemispherical coverage (scan to 90°) can be achieved with some minor mechanical scanning. To minimize the impact and design complexity, the antenna array integrates both the transmit and receive functionality. The prototype array presented in this paper is based on the design introduced in [4] and then improved in [5]. Here we present for the first time the experimental validation and we report the measured results obtained during the testing campaign. The differences in terms of requirements and capabilities between this array and the one in [4] are highlighted in Tab. I.

The antenna array is based on the connected array concept, formally introduced in [6] and theoretically further developed in [7]. Some of the present authors have continued to work on this concept in [4], [8]–[10]. Examples of design, although referred to as tightly coupled elements [11], can be found in [12], [13]. In a connected array, the antenna elements are either electrically connected or strongly capacitively coupled, so that the array acts as a single antenna structure that is periodically fed. In separate antenna elements, the longitudinal currents are sinusoidal and strongly frequency dependent. Conversely, in a connected array configuration, the currents remain uniform on

Manuscript received Month DD, 2015; revised Month DD 2015. First published Month DD, YYYY; current version published Month DD, YYYY. This work was supported by the European Space Agency Advanced Antenna Concepts for Aircraft in Flight Entertainment under ESTEC Contract C19865.

R. J. Bolt, D. Deurloo and R. Grooters, are with the Radar Technology Department of TNO, 2597 AK The Hague, The Netherlands (e-mail: roland.bolt@tno.nl).

G. Gerini is with the Optics Department of TNO, Stieltjesweg 1, 2628 CK Delft, The Netherlands and also the Faculty of Electrical Engineering, Eindhoven University of Technology, 5612 AZ Eindhoven (e-mail: giampiero.gerini@tno.nl).

D. Cavallo and A. Neto are with the Microelectronics Department, Delft University of Technology, 2628 CD Delft, The Netherlands (e-mail: d.cavallo@tudelft.nl, a.neto@tudelft.nl).

G. Toso is with the Electromagnetics Division, European Space Agency, 2200 AG Noordwijk, The Netherlands (e-mail: Giovanni.Toso@esa.int).

Color versions of one or more of the figures in this paper are available online at http://ieeexplore.ieee.org.

Digital Object Identifier XX.XXXX/TAP.XXXX.XXXXXXXX.

TABLE I
COMPARISON BETWEEN THE PRESENT DESIGN AND THE ARRAY IN [4].

	Design in [4]	Present design
Operational bandwidth	3 to 5 GHz	10.7 to 14.5 GHz
Polarization	Single	Dual
Maximum scan angle	45°	60°
Number of elements	$7 \times 7 = 49$	$16 \times 16 \times 2 = 512$

the entire array and nearly constant with frequency. Besides the wide bandwidth, connected arrays also provide high cross-polarization suppression, which is an important requirement for the application at hand and should be better than 15 dB [1]. For the generation of the radiation pattern, ETSI [14] and ITU [15] recommendations were considered. These altogether define a power density mask to prevent interference with other satellites and ground-based stations. While on the one hand the mask limits the maximum allowable beam width and side lobe level, on the other hand there is the need to push the antenna gain such that a maximum number of identical clients can concurrently make use of the service with an as high as possible data rate. In practice this boils down to an optimization of the amplitude tapering in combination with antenna size. Such an optimization resulted in an array of 70×70 dual-polarized cells with a raised cosine (−4.6 dB) amplitude tapering, which renders an adequate data rate between 49 Mbps (148 identical users) and 14 Mbps (42 identical users), respectively at broadside and for 60° of scan [1]. To experimentally validate the designed array, we did not construct the full sized array, but a scaled version (16×16 cells), eventually taking into account the consequent scaling of the pattern characteristics.

II. Array Prototype

A. Unit Cell Design

The array unit cell is depicted in Fig. 1. It consists of two orthogonal dipoles to attain the dual-polarization capability. The dipoles are printed on multi-layer vertical printed circuit boards (PCBs), where slots are cut out for orthogonally interleaving the two sets of elements, as shown in Fig. 2.

The unit cell measures 9×9 mm^2 which is equivalent to 0.435×0.435 λ_0^2 at the highest frequency of interest. As shown in Fig. 1(a), the vertical PCBs are intersected by two horizontal layers: a metal sheet acts as a backing reflector, for ensuring unidirectional radiation, and a thin dielectric layer implements a wide angle impedance matching (WAIM) sheet [16], for improving the scan performance. The practical implementation of the reflector and the WAIM sheets will be described in the following section. The dipoles are capacitively loaded at their edges to compensate for the inductive effect imposed by the ground plane [11]. The capacitance is implemented by printing the two arms of each dipole on two different layers of the PCB and by overlapping the arms of neighboring dipoles, as shown in Fig. 1(b). The final stack contains three Duroid RT5880 127 μm thick substrates and two RO2929 very thin (38 μm) bonding films, as depicted in the inset of Fig. 1(b).

Design aspects of the array have extensively been treated in [4], [8]–[10], and as such the design process will not

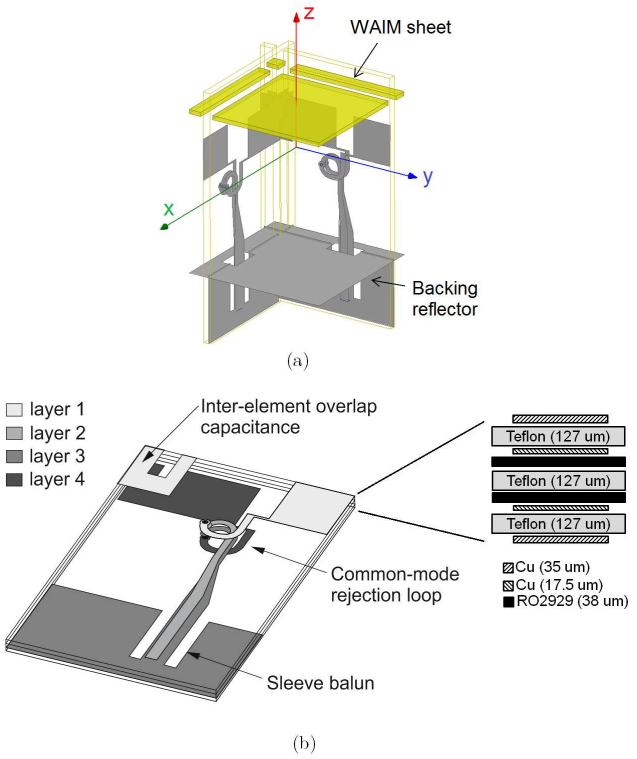

Fig. 1. (a) Three dimensional view of the array unit cell and (b) components of the dipole and the feed structure in the multi-layer printed circuit board.

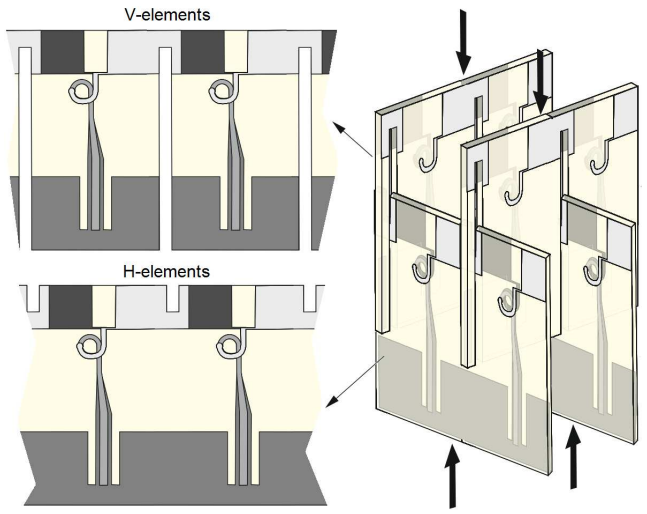

Fig. 2. Horizontally (H) and vertically (V) polarized antenna elements with cutouts for interleaving.

be repeated here. A difference with respect to earlier array designs, which operate at lower frequency regimes than the current one (S- and X-band), is related to the common-mode rejection loop. This loop has the purpose of improving cross-polarization suppression and overall efficiency [4]. In case of the current Ku-band design, we implement the loop using broadside coupled strip lines instead of co-planar ones, as represented in Fig. 3. The standard two-layer PCB technology is replaced by a four-layer (layer refers to copper) design to

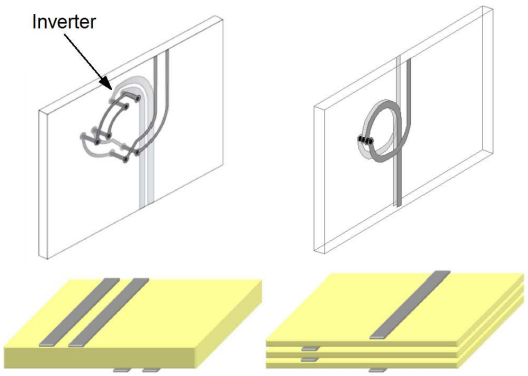

Fig. 3. Different loop concepts to reject the common-mode: (a) two-layer design based on co-planar strip lines including inverters and (b) four-layer design based on parallel strip lines.

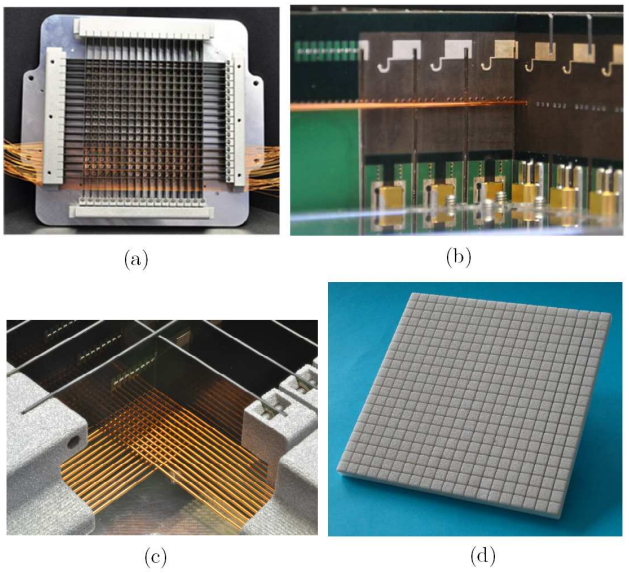

Fig. 4. Some steps in the construction of the prototype array: (a) fixed and interleaved antenna panels and weaving of the ground wires; (b) illustrative view on partly assembled hardware, with SMP inline connectors and orthogonal interleaving of antenna panels; (c) surface mount resistors to gradually absorb the edge currents and wire-grid reflector; (d) cover containing the WAIM-sheet.

accommodate this loop. Its design, as shown in Fig. 3(b), does not require inverters to maintain equal path lengths between the individual traces of the differential line, as the old design in Fig. 3(a). In fact, the matching performance of these inverters showed to degrade at higher frequency (Ku), due to the minimum dimensions of track and gap width allowed by the PCB technology.

B. Array Manufacturing

A view of the produced antenna prototype is presented in Fig. 4. The dimensions of a single vertical antenna panel are 210×30 mm^2. Figures 4(a) and (b) show intermediate steps during construction of the demonstrator array. The integration of the ground plane (reflector) by means of a wire grid

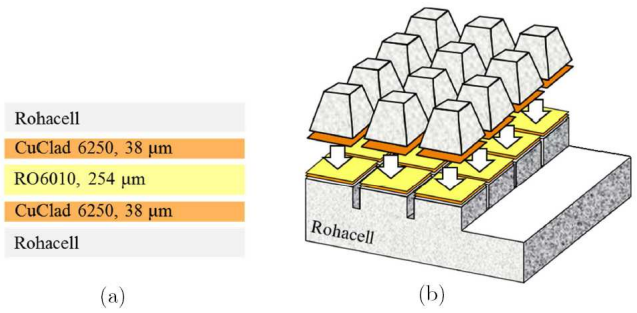

Fig. 5. (a) Implemented layer stack of the WAIM cover and (b) schematics of the WAIM realization steps.

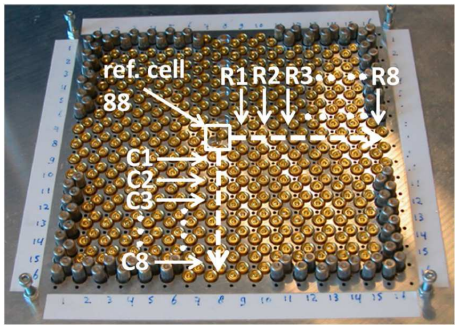

Fig. 6. Prototype backside, with highlighted the reference cell at row 8, column 8, and the other probed elements along the near-central horizontal direction (R#) and the near-central vertical direction (C#).

[4] includes 6×6 orthogonally inserted wires per cell. The procedure to manufacture the ground plane appeared to be well controllable and scalable to larger arrays, with obvious increase in assembly time. The total size of the array is 150×150 mm^2, and 265×265 mm^2 including the supporting flange. For each polarization, 16 functional multilayer PCBs are kept in place by a spring system, see details in Fig. 4(c).

As previously mentioned, the array is loaded with a WAIM-sheet. This sheet is characterized as electrically thin and of a high permittivity value [16]. For proper performance the sheet is positioned above the dipoles at about one-tenth of the smallest wavelength (λ_{min}) in the frequency band of interest. Its practical implementation is presented in Fig. 4(d). To guarantee the placement of the thin sheet at $\lambda_{\text{min}}/10$ from the dipoles, the ideally continuous sheet is segmented into small squares that just fit in the unit cells of the array. Correct and equal height position of the squares in each cell could effectively be established by integrating the sheet with a tailored foam cover. The WAIM-sheet layer stack is presented in Fig. 5(a) and is composed of Rohacell foam, CuClad 2650 bonding film and a RO6010 (ε_r =10.5) sheet. The manufactured WAIM cover is presented schematically in Fig. 5(b). Dimensions of the individual segments are slightly less than the cell sizes. The edged foam top-portions help to guide the square sheet segments in each of the array cells when mounting the cover onto the array. It was found in practice that mounting the WAIM cover on top of the array was a simple and repeatable process.

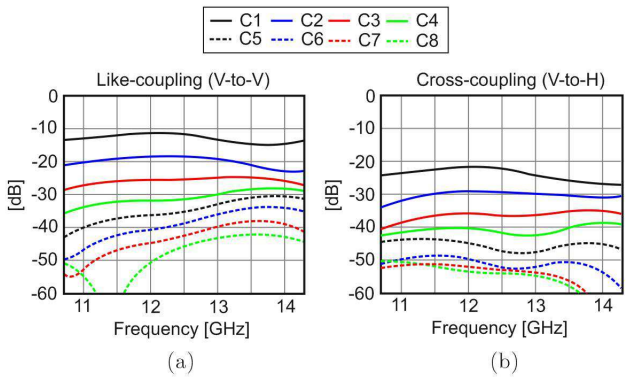

Fig. 7. Decay in the coupling levels measured along the vertical direction as indicated in Fig. 6, for the case of coupling between (a) like oriented and (b) orthogonal oriented elements.

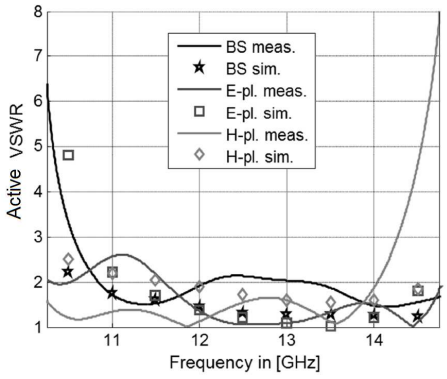

Fig. 8. Active VSWR as a function of frequency and scanning condition as indicated in the inset (BS = broadside, others: 60°). The array is fully excited.

III. Measurement of Matching Characteristics

A finite-element-method (FEM) modeler [17] has been used to simulate the present connected-dipole array, using the unit-cell approach. For optimum experimental validation of the simulated performance, logically the most centralized cell in the array is taken as a reference. All necessary coupling coefficients are thus probed and measured relative to this cell, which is indicated in Fig. 6.

A. Mutual Coupling and Active Matching

The coupling levels with increasing distance between active and probed elements has been explored. This was done along the horizontal and vertical directions as presented in Fig. 6. Each cell contains a horizontally (H) and a vertically (V) polarized element. The VV- and HV-couplings related to the designations $C_1 ... C_8$ in Fig. 6, are shown in the graphs of Fig. 7. We can observe individual smooth behaviors (absence of sharp resonances), non-overlapping curves and a gradual decay with increasing inter-element distance. Similar graphs exist for the remaining couplings (HH and VH), but they are not reported for the sake of brevity.

The active VSWR is plotted in Fig. 8 for broadside (BS) and radiation under extreme scanning conditions (60° in the E- and H-plane). These results refer to the sum of 11×11 elements centered on the reference cell '88' (see Fig. 6). Both polarizations of the array are active. Summing a subset of the entire array for the calculation of the active impedance leaves two or three rows of dummy elements at the edges of the array.

From the shown cases, the comparison of the measured AR with simulations is appreciable. Since the prototype is a complex structure, deviations can be attributed to tolerances in the production process. We have considered a number of tolerances inherent to the structure and found effects that can explain the indicated deviations.

Based on the acquired coupling database, the AR has also been calculated for an extended set of scan conditions. These range through the complete scanning cone of interest, i.e.: $\theta_s = \{0°, ..., 60°\}$ for all planes $\phi_s = \{0°, ..., 360°\}$. Results are presented in Fig. 9 for two frequencies in the receive band, 11 and 12 GHz, and one frequency in the transmit band, 14.25 GHz. The active reflection coefficient is plotted as a function of the scan direction cosines, i.e.: (u_s, v_s) for which we then have: $(u_s^{\max}, v_s^{\max}) = \sin 60° = \sqrt{3}/2$ as the maximum scan radius of interest. The maps refer to horizontal polarization and, as expected, we found an orthogonal symmetry when comparing with the vertical polarization. From the graphs on the active reflection coefficient, we can observe that in some specific situations its value approaches -5 dB. Especially in the receive band (10.70 to 12.75 GHz) this might be considered as problematic. However, such a level can be tolerated by the application at hand where the required receive chain sensitivity is 8 dB/K.

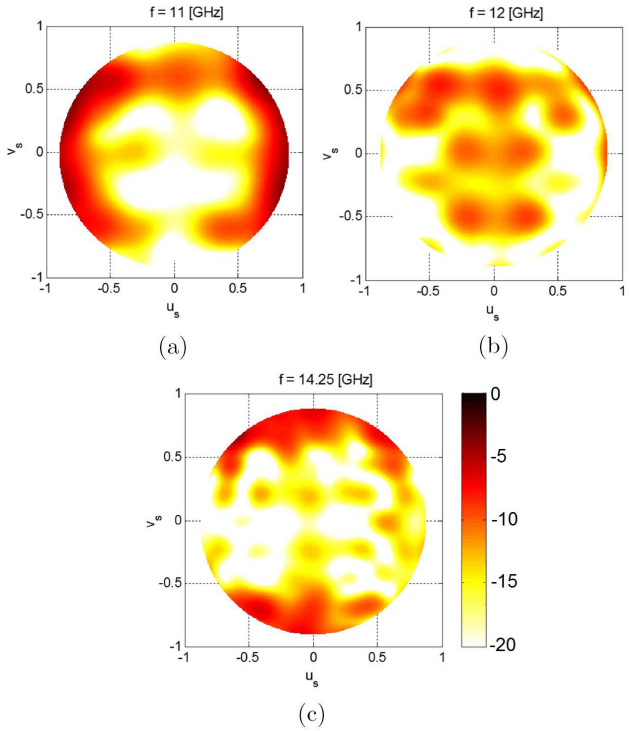

Fig. 9. Measured active reflection coefficient for the complete scanning range at different frequencies. Two frequencies in the receive band (a), (b), and one in the transmit band (c).

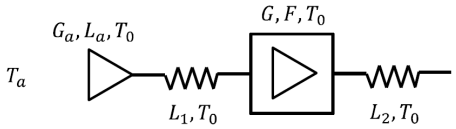

Fig. 10. Receive chain schematic indicating, in addition to losses mentioned in the text, losses in the feed network L_1 and the network beyond the LNA L_2.

B. System Sensitivity

Antenna matching levels, active or not, are mostly considered as good when they are lower than -10 dB. However, the qualification "good" depends on the requirements of the application. For the current case, a system gain over effective system temperature (G_{SYS}/T_e) of 8 dB/K is required.

Considering a receive chain containing a low noise amplifier (LNA, see Fig. 10) with sufficiently high gain and noise figure F, the following expression can be written:

$$\frac{G_{\mathrm{SYS}}}{T_e} = \frac{(1-|\Gamma|^2)G_a}{T_a\left((1-|\Gamma|^2)+\frac{T_0}{T_a}(FL-1)\right)}. \qquad (1)$$

In (1) the antenna array gain is represented by G_a, $L = L_a L_1$ is the combined attenuation due to material losses of the antenna ($L_a > 1$) and feed network ($L_1 > 1$), and Γ is the active reflection coefficient of the unit-cell element. The combined material losses at Rx have been calculated as 0.75 dB (worst case, simulated with HFSS for a unit cell [17]), and T_a for an antenna with no earth-directed side lobes is estimated at 50 K. Additionally, we have $T_0 = 290$ K. For the antenna array envisaged for the application 70×70 elements are required, which give a gain of 36.45 dBi at 10.7 GHz, when scanning to 60°.

To get an indication of the worst acceptable Γ for the current application, we can set $G_{\mathrm{SYS}}/T_e = 8$ dB/K and invert Eq. (1) to find the noise figure of the LNA as a function of the active reflection. This analysis, shown in Fig. 11, indicates that moderate matching levels can be accepted without need for unrealizable receive chain noise figures. For instance, an active reflection coefficients of -5 dB would still satisfy the requirement on the G_{SYS}/T_e if the receive chain noise figure is about 3.2 dB. Such noise figure can be guaranteed by nowadays off-the-shelf components.

C. Dependence on Polarization

For the current application, specific polarization settings are required depending on the operational mode. In the receive mode the polarization must be circular, either RHCP or LHCP. In the transmit mode the polarization must be variable slant linear.

The effect of the polarization on the AR has been calculated for BS and beam scans towards 60° as visualized in the graph of Fig. 12. For all the polarization settings equal amplitude is considered for the two orthogonal arrays. It is observed that the variation of the active VSWR for the polarization setting is quite contained throughout the frequency range. Similar variations can be expected for other beam settings.

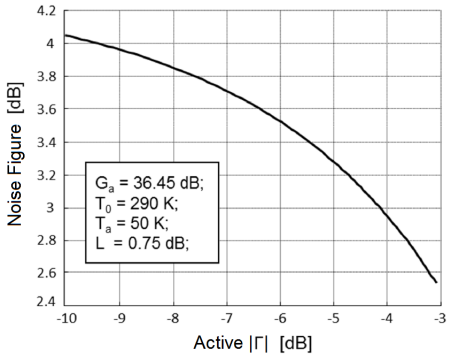

Fig. 11. Required noise figure of the LNA as a function of the array active reflection coefficient.

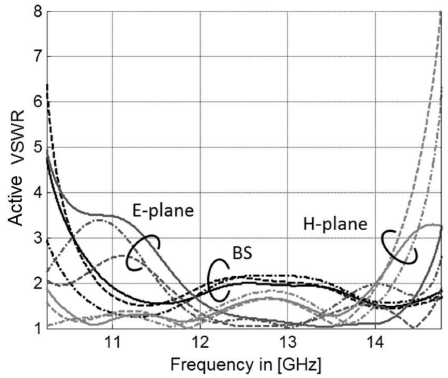

Fig. 12. Dependency of the measured active VSWR on the polarization setting. The beam has been scanned in three different directions: BS (broadside, black), E-plane (darkgrey), and H-plane (light-grey). Three polarization states have been implemented: LHCP (solid lines), 45° slant polarization (dashed lines) and RHCP (dash-dotted lines).

IV. Radiation Characteristics

In order to characterize the realized array also at pattern level, specific test support equipment (TSE) has been developed. In Fig. 13, a view on the realized TSE architecture is shown. The TSE is a programmable passive beam former network (BFN) that utilizes a mother board to drive 16 daughter boards. Each of these daughter boards comprises 32 analog phase shifters for beam direction control, and 32 analog attenuators to control the amplitude tapering. These components are equally divided over both sides of the boards. Polarization control is arranged at mother board level by adjusting the amplitude and phase in both main branches.

A comparison between the measured and simulated radiation patterns for scanning to $\theta_s = \{30°, 60°\}$ in the H-plane and D-plane is shown in the graphs of Figs. 14 and 15 respectively. The patterns that were measured for scanning in the E-plane are quite similar to those of the H-plane and have therefore not been included. Simulations refer to the infinite array analysis performed in Ansys HFSS [17], to which a windowing approximation is applied [18] to include the array factor. All patterns in the graphs are normalized to the maximum level at 30° scan and relate to the highest frequency considered in the receive band (12.1 GHz). Especially from

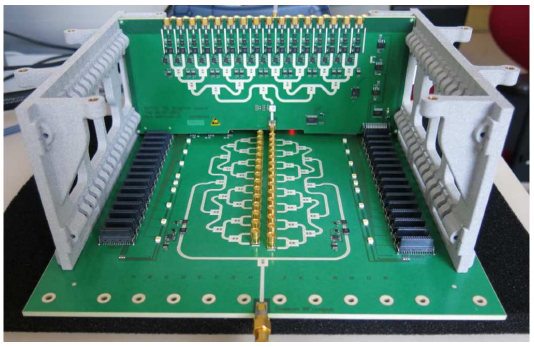

Fig. 13. Photograph of the partly assembled TSE. The horizontal panel is the mother board on which the RF power is divided to the two orthogonal polarized arrays. The vertical panel is one of the 16 daughter boards feeding a row of 16 dual-polarized cells.

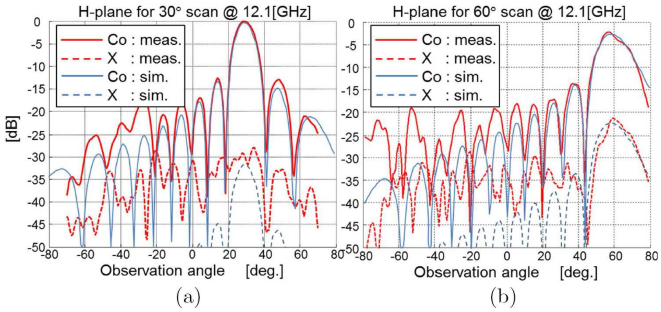

Fig. 14. Comparison between the measured and simulated patterns scanned in the H-plane, i.e.: scanned to $(\phi_s, \theta_s) = (90°, 30°)$ and $(90°, 60°)$ in (a) and (b) respectively. Similar patterns were observed in the E-plane, i.e.: scanned to $(\phi_s, \theta_s) = (0°, 30°)$ and $(0°, 60°)$ respectively.

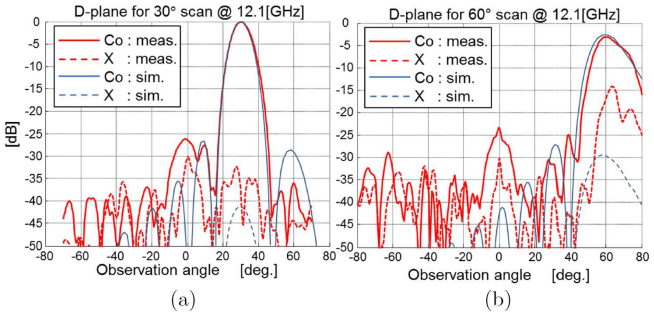

Fig. 15. Comparison between the measured and simulated patterns scanned in the D-plane, i.e.: scanned to $(\phi_s, \theta_s) = (45°, 30°)$ and $(45°, 60°)$ in (a) and (b) respectively.

the results in the principal plane, the pattern shows well-defined main beam, nulls and side lobe decay. Co- and cross-polarized patterns compare well to simulations. First side lobe amplitudes for broadside radiation were found close to the -13.27 dB level for uniform illumination and the widening of the main beam over scan angle follows the $1/\cos\theta$ rule. In the diagonal plane, cross-polar levels (defined according to the third definition of Ludwig [19]) are higher than the expectation from simulations. However the values are below 10 dB.

Since the worst cross-polarization levels can be expected along the diagonal plane it is of special interest to observe

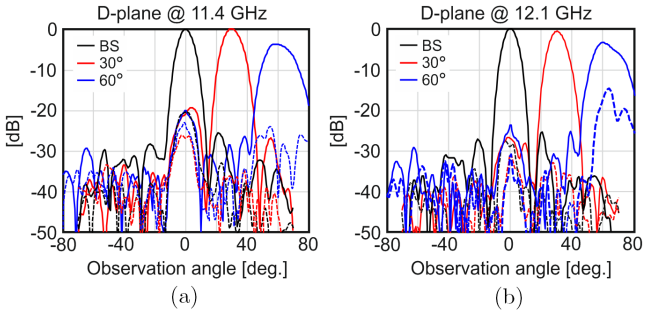

Fig. 16. Measured co- (solid lines) and cross-patterns (dashed lines) scanned in the D-plane, i.e.: scanned to $(\phi_s, \theta_s) = (45°, \{0°, 30°, 60°\})$ at (a) 11.4 GHz and (b) 12.1 GHz. BS indicates broadside.

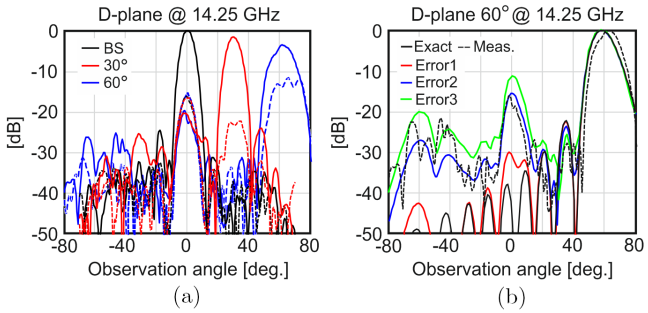

Fig. 17. (a) Measured co- (solid lines) and cross-patterns (dashed lines) scanned in the D-plane to $\theta_s = \{0°, 30°, 60°\}$ at 14.25 GHz. BS indicates broadside; (b) effects of TSE amplitude and phase errors on the patterns. The colored curves relate to patterns that include errors in the amplitude and phase distribution. Largest errors relate to the green curve and the smallest errors to the red curve. The blue curve represents the pattern when the simulated errors match those measured on the TSE in a stand-alone condition.

the pattern characteristics for those situations. Broadside and scanned patterns for the three frequencies are plotted in the graphs of Figs. 16 and 17. Again, also here the expected features of the radiation pattern can be distinguished, such as low side lobes and beam widening for larger scan angles. Cross-polarization levels remain quite low except for the extreme scanning angle at the higher frequencies.

Less obvious for the principal plane but clearly identifiable for the diagonal plane patterns (where the side lobes are on average at a significant lower level) is a distinctive lobe at broadside for both the co- and cross-polarized patterns. A specific study related to this has shown that it is induced by the imperfections generated by the TSE. This is indicated in Fig. 17(b) where the measured pattern for extreme scanning in the plane at the highest frequency is compared to patterns calculated through a rigorous summation of cosine element patterns. These elements are placed with the same periodicity of the prototype array but fed with several erroneous phase and amplitude distributions derived from the practical settings of the BFN. Obviously, when lowering the error, the pattern will eventually line up with the exact one. Deviations reaching an absolute error as high as 10° in phase and an average error of -1.3 dB in power (represented by the blue curve) with respect to the ideal distributions, induce the broadside lobe that is comparable to the one measured. These deviations were

also found during characterization of the TSE in a stand-alone condition after comparing the generated aperture distribution with the ideal distribution.

V. Conclusions

A Ku-band dual-polarized connected dipole array consisting of 512 elements has been successfully constructed and tested. The prototype array is characterized both in terms of active reflection and radiation characteristics. It was found that the reflection is compliant with the required G_{SYS}/T_e of 8 dB/K for the application. Comparison of the experimental results with simulations shows to be appreciable and deviations can mainly be attributed to tolerances in the manufacturing process.

By means of the developed BFN we have been able to test the radiation characteristics of the prototype array for several scanning conditions. The resulting measured patterns indicate good performance and good match with the simulated patterns. For the vast majority of cases the measured cross-polarization suppression reached levels higher than 15 dB. Only for the higher frequencies under extreme scanning the cross-polar suppression reduces to 10 dB. The antenna can scan electronically up to 60° in all azimuth planes.

Acknowledgments

The authors wish to express their appreciation for the craftsmanship of the TNO The Hague workshop, which to a large portion contributed to the successful completion of the performed work. All the work presented in this paper has been performed under an ARTES 5.1 contract.

References

[1] R. Grooters, G. Gerini, A. Neto, R. Bolt, and D. Cavallo, "ACTiFE Phase 2, System/demonstrator definition of a single panel connected array antenna," European Space Agency, Noordwijk, The Netherlands, Tech. Rep. 21, WP2100, ESA Contract no. 4000101757, Feb. 2011.

[2] E. B. Felstead, "A perspective on future naval sitcom antennas," *Military Communications Conference*, 2005.

[3] A. Catalani, F. Di Paolo, M. Migliorelli, L. Russo, G. Toso and P. Angeletti, "Ku band hemispherical fully electronic antenna for aircraft in-flight entertainment," *International Journal of Antennas and Propagation*, vol. 2009, Article ID 230650, 7 pages, 2009. doi:10.1155/2009/230650

[4] D. Cavallo, A. Neto, G. Gerini, A. Micco, and V. Galdi, "A 3 to 5 GHz wideband array of connected dipoles with low cross polarization and wide-scan capability," *IEEE Trans. Antennas Propag.*, vol. 61, no. 3, pp. 1148-1154, Mar. 2013.

[5] D. Cavallo, G. Gerini, R. J. Bolt, D. Deurloo, R. Grooters, A. Neto, G. Toso, and R. Midthassel, "Ku-band dual-polarized array of connected dipoles for satcom terminals: Theory and hardware validation," *Eur. Conf. Antennas Propag.*, Gothenburg, Sweden, Apr. 8-12, 2013.

[6] R. C. Hansen, "Linear connected arrays," *IEEE Antennas Wireless Propag. Lett.*, vol. 3, pp. 154-156, 2004.

[7] A. Neto and J. J. Lee, "Ultrawide-band properties of long slot arrays," *IEEE Trans. Antennas Propag.*, vol. 54, no. 2, pp. 534-543, Feb. 2006.

[8] A. Neto, D. Cavallo, G. Gerini, G. Toso, "Scanning performance of wideband connected arrays in the presence of a backing reflector, *IEEE Trans. Antennas Propag.*, vol. 57, no. 10, pp. 3092-3102, Oct. 2009.

[9] A. Neto, D. Cavallo, G. Gerini, "Edge-born waves in connected arrays: A finite infinite analytical representation," *IEEE Trans. Antennas Propag.*, vol. 59, no. 10, pp. 3646-3657, Oct. 2011.

[10] D. Cavallo, A. Neto, and G. Gerini, "Analytical description and design of printed dipole arrays for wideband wide-scan applications," *IEEE Trans. Antennas Propag.*, vol. 60, no. 12, pp. 6027-6031, Dec. 2012.

[11] B. A. Munk, *Finite Antenna Array and FSS.*, John Wiley & Sons, Inc., Hoboken, NJ, USA, 2003.

[12] W. F. Moulder, K. Sertel, and J. L. Volakis, "Ultrawideband superstrate-enhanced substrate-loaded array with integrated feed," *IEEE Trans. Antennas Propag.*, vol. 61, no. 11, pp. 5802-5807, Nov. 2013.

[13] S. S. Holland and M. N. Vouvakis, "The planar ultrawideband modular antenna (PUMA) Array," *IEEE Trans. Antennas Propag.*, vol. 60, no. 1, pp. 130-140, Jan. 2012.

[14] ETSI EN 302 186 V1.1.1 (2004-01), "Satellite Earth stations and systems (SES); Harmonized EN for satellite mobile Aircraft Earth Stations (AESs) operating in the 11/12/14 GHz frequency bands covering essential requirements under article 3.2 of the R&TTE Directive".

[15] Recommendation ITU-R M.1643, "Technical and operational requirements for aircraft earth stations of aeronautical mobile-satellite service including those using fixed-satellite service network transponders in the band 14-14.5 GHz (Earth-to-space)," 2003.

[16] E. G. Magill and H. A. Wheeler, "Wide-angle impedance matching of a planar array antenna by a dielectric sheet," *IEEE Trans. Antennas Propag.*, vol. AP-14, no.1, Jan. 1966.

[17] ANSYS HFSS v14, ANSYS, Inc., Canonsburg, PA, [Online.] Available: http://www.ansys.com/.

[18] A. Ishimaru, R. Coe, G. Miller, and W. Geren, "Finite periodic structure approach to large scanning array problems," *IEEE Trans. Antennas Propag.*, vol. 33, no. 11, pp.1213-1220, Nov. 1985.

[19] A. C. Ludwig, "The definition of cross polarization, *IEEE Trans. Antennas Propag.*, vol. AP-21, no. 1, pp. 116-119, Jan. 1973.

Roland Bolt received his ... .

Since, from, he was... His research interests include ...

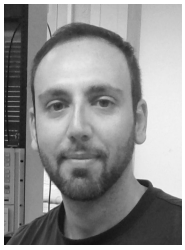

Daniele Cavallo (S'09−M'11) received the M.Sc. degree (*summa cum laude*) in telecommunication engineering from the University of Sannio, Benevento, Italy, in 2007, and his Ph.D. degree (*cum laude*) in electromagnetics from Eindhoven University of Technology (TU/e), Eindhoven, Netherlands, in 2011.

From 2007 to 2011, he was with the Antenna Group at the Netherlands Organization for Applied Scientific Research (TNO), The Hague, Netherlands. In the years 2012-2015, he was Post-Doctoral researcher in the Microelectronics department of Delft University of Technology (TUDelft), Delft, Netherlands. During 2015, he spent two months as a visiting researcher at Chalmers University of Technology in Gothenburg, Sweden. From September 2015, he is assistant professor in the Terahertz Sensing Group at TUDelft. He is the author or coauthor of more than 70 papers published in peer-reviewed international journals and conference proceedings. His research interests include analytical and numerical methods for antenna characterization, the design of antenna arrays and high-frequency on-chip antennas.

Dr. Cavallo was first author of the paper awarded with the best innovative paper prize at the 30th ESA Antenna Workshop in 2008 and nominee for the best doctoral project in the TU/e Academic Annual Awards 2012. He has been awarded a three-year personal grant from the Netherlands Organization for Scientific Research (NWO VENI, 250 keuro), for developing "Efficient On-Chip Antennas for Terahertz Applications". He is a member of the European Association on Antennas and Propagation (EurAAP).

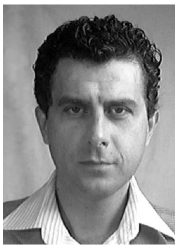

Giampiero Gerini (M'92−SM'08) received the M.Sc. degree (*summa cum laude*) and the Ph.D. degree in electronic engineering from the University of Ancona, Italy, in 1988 and 1992, respectively.

From 1992 to 1994, he was Assistant Professor of electromagnetic fields at the same university. From 1994 to 1997, he was Research Fellow at the European Space Research and Technology Centre (ESA-ESTEC), Noordwijk, The Netherlands, where he joined the Radio Frequency System Division. Since 1997, he has been with the Netherlands Organization for Applied Scientific Research (TNO), The Hague, The Netherlands. At TNO Defence Security and Safety, he is currently Chief Senior Scientist of the Antenna Unit in the Transceiver Department. In 2007, he was appointed as part-time Professor in the Faculty of Electrical Engineering of the Eindhoven University of Technology, Eindhoven, The Netherlands, with a Chair on Novel Structures and Concepts for Advanced Antennas. His main research interests are phased arrays antennas, electromagnetic bandgap structures, frequency-selective surfaces and integrated antennas at microwave, and millimeter and sub-millimeter wave frequencies. The main application fields of interest are radar, imaging, and telecommunication systems.

Prof. Gerini was corecipient of the 2008 H. A. Wheeler Applications Prize Paper Award of the IEEE Antennas and Propagation Society. He was corecipient also of the Best Innovative Paper Prize of the Thirtieth ESA Antenna Workshop in 2008 and of the Best Antenna Theory Paper Prize of the European Conference on Antennas and Propagation (EuCAP) in 2010.

Andrea Neto (M'00−SM'10−F'16) received the Laurea degree (*summa cum laude*) in electronic engineering from the University of Florence, Florence, Italy, in 1994 and the Ph.D. degree in electromagnetics from the University of Siena, Siena, Italy, in 2000.

Part of his Ph.D. degree was developed at the European Space Agency Research and Technology Center, Noordwijk, The Netherlands, where he worked for the antenna section for over two years. In the years 2000−2001, he was a Post-Doctoral Researcher at the California Institute of Technology, Pasadena, CA, USA, working for the Sub-Millimeter-Wave Advanced Technology Group. From 2002 to January 2010, he was a Senior Antenna Scientist at TNO Defence, Security, and Safety, The Hague, The Netherlands. In February 2010, he was appointed Full Professor of Applied Electromagnetism in the Electrical Engineering, Mathematics and Computer Science Department, Technical University of Delft, Delft, The Netherlands, where he formed and leads the THz Sensing Group. His research interests are in the analysis and design of antennas, with emphasis on arrays, dielectric lens antennas, wideband antennas, EBG structures, and THz antennas.

Prof. Neto was corecipient of the H. A. Wheeler award for the best applications paper of the year 2008 in the IEEE TRANSACTIONS ON ANTENNAS AND PROPAGATION. He was corecipient of the best innovative paper prize at the 30th ESA Antenna Workshop in 2008. He was corecipient of the best antenna theory paper prize at the European Conference on Antennas and Propagation (EuCAP) in 2010. He served as an Associate Editor of the IEEE TRANSACTIONS ON ANTENNAS AND PROPAGATION (2008−2013) and IEEE ANTENNAS AND WIRELESS PROPAGATION LETTERS (20052013). He is member of the Technical Board of the European School of Antennas and organizer of the course on Antenna Imaging Techniques. He is a member of the steering committee of the network of excellence NEWFOCUS, dedicated to focusing techniques in mm and sub-millimeter-wave regimes. In 2011 he was awarded the European Research Council Starting Grant to perform research on Advanced Antenna Architectures for THz Sensing Systems.

Duije Deurloo received his ... .

Since, from, he was... His research interests include ...

Reindert Grooters received his ... .

Since, from, he was... His research interests include ...

Giovanni Toso (S'93−M'00−SM'07) received the Laurea degree (*summa cum laude*) and the Ph.D. degree in electrical engineering from the University of Florence, Florence, Italy, in 1992 and 1995, respectively.

In 1996, he was a Visiting Scientist at the Laboratoire dOptique Electromagnétique, University of Aix-Marseille III, Marseille, France. From 1997 to 1999, he was a Postdoctoral Student at the University of Florence, Firenze, Italy. In 1999, he was a Visiting Scientist at the University of California, Los Angeles (UCLA), CA, USA. In the same year, he received a scholarship from Thales Alenia Space (Rome, Italy) and was appointed Researcher with the Radioastronomy Observatory of the Italian National Council of Researches (CNR). Since 2000, he has been with the Antenna and Submillimeter Section, European Space and Technology Centre, European Space Agency, ESA ESTEC, Noordwijk, The Netherlands. He has been initiating and contributing to several R&D activities on satellite antennas based on arrays, reflectarrays, constrained lenses and reflectors. He has coauthored more than 50 technical papers published in peer-reviewed professional journals, more than 200 papers published in international conference proceedings, and more than 10 international patents. In 2009, he was the Co-Editor of the Special Issue on Active Antennas for Satellite Applications in the *International Journal of Antennas and Propagation.*

Dr. Toso has been the Co-Guest Editor of the Special Issue on Innovative Phased Array Antennas Based on Non-Regular Lattices and Overlapped Subarrays published in the IEEE TRANSACTIONS ON ANTENNAS AND PROPAGATION in April 2014. He is an Associate Editor of the IEEE TRANSACTIONS ON ANTENNAS AND PROPAGATION.